Mathematical Model of the Solid Flow Behavior in a Real Dimension Blast Furnace

Reza Safavi Nick

Licentiate Thesis

Stockholm 2012

Division of Applied Process Metallurgy
Department of Materials Science and Engineering
KTH Royal Institute of Technology
SE-100 44 Stockholm
Sweden

Akademisk avhandling som med tillstånd av Kungliga Tekniska Högskolan i Stockholm, framlägges för offentlig granskning för avläggande av Teknologie Licentiatexamen, tisdagen den 4 december 2012, kl. 10.00 i Sefström konferensrum, Brinellvägen 23, Kungliga Tekniska Högskolan, Stockholm, Sweden.

Reza Safavi Nick: **Mathematical Model of the Solid Flow Behavior in a Real Dimension Blast Furnace**

Division of Applied Process Metallurgy
Department of Materials Science and Engineering
School of Industrial Engineering and Management
Royal Institute of Technology
SE-100 44 Stockholm
Sweden
ISBN 978-91-7501-560-6

Computers are useless. They can only give you answers.

Pablo Picasso

Intentionally left blank!

Abstract

A mathematical model based on the continuum mechanic concept has been developed to describe the profile of solid particles in an industrial scale blast furnace. The focus is the in-furnace conditions and its characteristics such as the shape and size of the deadman. The Navier-Stokes differential equation for multi-phase multi-dimensional space has been used to describe the behavior of existing phases. The equation has been modified to make it possible to describe the dual nature of the solid phase in the system. This has been done by applying the concept of the solid surface stress to describe the inter-granular surface interactions between particles. More specifically, this term is added as an extra term to the Navier-Stokes equation to describe the particle-particle interactions. This extra term in behave as a breaking force when the particles are sliding down in the furnace. During the descending movement in the furnace it is shown that the particles change their profile from a V-shape to a W-shape, due to the characteristics of the deadman. Moreover, the velocity magnitude is higher at the outer surface of the deadman for higher grid-slabs in this region than the near-wall cells. However, the situation changes as solid particles moving to even lower levels of the grid-slabs at the outer surface of the deadman in comparison to near-wall cells. It has also been shown that an increase in the magnitude of the effective pressure reduces the velocity magnitude of descending particles. Furthermore, since different phases co-exist in a blast furnace, the volume fraction plays an important role in the blast furnace. Therefore, the influence of three different packing densities (0.68, 0.71 and 0.74 respectively) on the profile of the flow through the upper part of the blast furnace from the throat to the tuyeres level has been studied. It is shown that an increase in the volume fraction of the solid phase lead to a decrease in the velocity magnitude. This decrease is due to an increase in the solid volume fraction, which will increase the resident time of the particles inside a blast furnace. In addition, it is shown that the velocity magnitude of the solid phase decreases from the throat to the belly of the furnace, for the studied conditions. However, after belly the velocity magnitude increases again.

Intentionally left blank!

Acknowledgements

At first, I would like to express my deepest gratitude to my supervisors Professor Pär Jönsson, Professor Lage Jonsson and Dr. Anders Tilliander for their guidance, support and open door policy. I would like to specifically thank Professor Pär Jönsson which I learned a lot from him how to improve myself and help others at the same time. I should also explicitly thank Professor Lage Jonsson which thought me a lot more than I could imagine. The support I received from my supervisor is hard to describe and will stay with me as long as I live.

I would also like to thank Professor Tatsuro Ariyama. It was a great experience to work in his laboratory at Tohoku University at Sendai, Japan.

I wish to thank Sweden-Japan Foundation, Axel Ax:son Johnsons, Stiftelsen Jernkontorsfonden for Bergsvetenskaplig forskning, Anders Henrik Göranssons Forskningsfond, Stiftelsen Prytziska Fonden, Stiftelsen Axel Hultgrens Fond and Jernkontoret which partly funded this study.

Of course, an important part of this acknowledgement goes to my friends at Royal Institute of Technology (KTH) and most of all, department of Materials Science and Engineering for all the fun I had and more importantly their patient! I should thank my friends at Sendai, Japan which we had lots of fun together. I would also like to express my gratitude to my other friends outside of the school for all the memorable moments I share with them. Because of you, my life was much easier and a lot more fun. You made it easy for me to live in another country far from my family and friends in Iran.

I like to take this opportunity and thank Jan-Olov Wikström and Jonas Alexis to give me a chance to be part of Swerea MEFOS AB. I also want to thank Jonas Alexis for the help I received during these last couple of months to manage to finish my thesis. I have to thank my friends there as well which made the transition time easy to me.

Finally, I want to thank my family in Iran. Even though we live far distant to each other, I always feel their support and endless love.

I believe this work should tribute to all of you as part of my appreciation for all the things I shared and experienced with you.

Stockholm, January 2012

Reza Safavi Nick

Intentionally left blank!

Supplements

The current work is based on the following supplements:

Supplement 1.

Mathematical Model of Solid Flow Behavior in a Real Dimension Blast Furnace

R. Safavi Nick, A. Tilliander, T.L.I. Jonsson and P. G. Jönsson

Submitted for publication to ISIJ International, September 2012

Supplement 2.

Mathematical Model of Solid Flow Behavior in a Real Dimension Blast Furnace: Effects of the Solid Volume Fraction on the Velocity Profile

R. Safavi Nick, A. Tilliander, T.L.I. Jonsson and P. G. Jönsson

Submitted for publication to Steel Research International, October 2012

Intentionally left blank!

List of Tables

Intentionally left blank!

List of Figures

Intentionally left blank!

Nomenclature

c	Compaction modulus	[-]
C_d	Drag coefficient	[-]
d_p	Particle diameter	[m]
D	Stretching tensor	[1/s]
$\vec{g}$	Gravity	[m/s^2]
G_0	Normalizing units factor	[-]
I	Identity matrix	[-]
p	Pressure	[Pa]
P_e	Effective pressure	[Pa]
Re_p	Particle Reynolds number	[-]
S	Source term	[kg/m^{2}s]
$\vec{u}$	Velocity vector	[m/s]

Greek letter

α_1	Cohesion	[-]
α_2	Friction coefficient	[-]
β	Gas-particle momentum transfer coefficient	[kg/m^3.s]
Γ	Effective diffusive transfer coefficient	[-]
ε	Volume fraction	[-]
ε_s^*	Volume fraction of solid particles (packing density)	[-]
η_s	Coefficient of plastic modulus	[-]
λ_p	Slip parameter	[m]
μ	Viscosity	[kg/m.s]
ρ	Density	[kg/m^3]
τ	Stress tensor	[kg/m.s^2]
Φ	General dependent variable (momentum: $\vec{u}_i$)	[-]
ϕ	Internal friction angle	[o]
φ_s	Sphericity of the particle	[-]

Subscripts

i	Phase index
g	Gas
s	Solid
ri	Rate-independent
rd	Rate-dependent

Intentionally left blank!

Table of Contents

Intentionally left blank!

1 Introduction

The blast furnace vessel is very complex operating systems in the field of process metallurgy. Even though the blast furnace process was assumed to be at its end during 80s, the rate of production of liquid iron by blast furnace increased dramatically during the last two decades.[1] This increment eventually spotlighted the blast furnaces as the main alternative in the ironmaking root in comparison to direct reduced iron DRI and other methods. Therefore, it is important to have a good understanding of the process and phenomena inside this metallurgical vessel. Meanwhile, the operational conditions and mostly the high temperature make it if not impossible, extremely difficult to retrieve any data from the in-furnace conditions for full scale operational blast furnaces. Hence, alternative methods for predicting the condition of in-furnace processes became the focus of numerous studies. Improvement in numerical methods and developments of computer hardware simultaneously, brought more attention to modeling of metallurgical processes. Consequently, mathematical models of blast furnaces have been developed to study and investigate the in-furnace phenomena.[2] Since early 90s, many mathematical models have been presented to illustrate the behavior of this vessel.[2-30]

In general, there are two major approaches in modeling of a blast furnace: continuum and discrete models. The continuum approach assumes that all the phases in the furnace behave like a continuum medium and is based on a local average principle.[3-21] On the other hand, the discrete method is based on Newton's second law of motion and is focused on the behavior of each and all individual particles in the system.[22-30] The discrete element method (DEM) is originally developed by Cundall and Strack [31] and is very effective to model granular materials. However, it is still very time-expensive to use this method for simulations of a blast furnace, even considering the development of computers hardware. One of these limitations is the number of particles that can be handled by the computers, which hardly would be comparable to the number of particles in an actual blast furnace in today's simulations.

The continuum method, as mentioned earlier, assumes that each phase in the system is a continuum medium. Therefore, the conservation equations can be used to model and predict the behavior of different phases which exists in the furnace. Since there are more than one medium in this process, a multi-phase model must be used. Thus, the conservation equations for each and all phases must be solved simultaneously, whilst the effect of each phase on other phases in the process must be taken into account. One of the benefits of this method is the simplicity of expanding a two-dimensional model to a three-dimensional model.

In addition to the methods described above, there are other attempts to model a blast furnace. One of these methods is based on the hypo-plasticity theory. This theory was developed at the University of Karlsruhe.[32, 33] However, there are not many reports on modeling a blast furnace based on the hypo-plasticity theory yet.[34-36]

It can be said that one of the most important phenomena in a blast furnace is the solid phase behaviour. Therefore, understanding the development of the profile of solid particles during the process could help to improve the solid particles charging method and the rate. In addition, solid interactions have direct effect on the gas and/or liquid injection. As a result, the quality and quantity of the outlet product and operational conditions of a blast furnace can be improved by improved knowledge of solid particle behaviour. **Table 1** shows a summary of published articles which focused on the solid flow modelling of blast furnaces since 1993. Chen *et al.* [4] was one the earlier who published a mathematical model of a blast furnace based on the continuum approach. In that article the solid phase was considered as a continuous media of a viscous fluid. Furthermore, the concept of solid viscosity was developed in the study to describe the friction between particles. In addition, the friction between solid particles and furnace wall and/or deadman boundary was expressed by Fanning type equations which was added as a source term to the Navier-Stokes equation. Moreover, the interaction force between gas and particles in their study was based on the Ergun's equation. Later, Austin *et al.* [5] presented a two-dimensional four-phase model of a blast furnace considering motion and heat transfer for all the existing phases. The model uses the viscous solids flow model proposed by Chen *et al.* [4] with an exception of the interphase drag force. In that study, Austin *et al.*[5] used the Ergun's equation in the anisotropic form to calculate the drag force in order to consider the differences between ore and coke layers. The Ergun's equation in the anisotropic form was used later on to model the interphase drag force.[5-8, 10-12] Thereafter, Austin *et al.* [6] presented an extension to their previous work [5] which solved the composition of all the phases, including compositional changes due to chemical reactions and the effects of such compositional changes on phase properties. In 1998, Austin *et al.* presented another article [7] with the purpose to extend and validate previously presented results of their model.[5, 6] In the same year, Zhang *et al.* [8] presented a model of a blast furnace based on continuum mechanics principle and Navier-Stokes equation. Moreover, it is said in their study that solid particles can either flow in a manner similar to a fluid media or being stagnant and providing a resistance to the particles movement. Therefore, they used the constitutive equations to describe this dual nature of the solid phase. Moreover, the Newtonian type of constitutive equation was used in that study to describe the viscous nature of the solid phase, while the dry Coulomb frictional relation was used to describe the other. Later on, in 2002 [14] Zhang *et al.* published another article based on the same concept. A year later, Takatani *et al.* [9] published a mathematical model of a blast furnace using a kinematic model to describe the solid flow in the furnace. Since the model considered the chemical reaction, the mass balance equation was modified so that it considered the reactions in the furnace. Castro *et al.* [10-13, 21] published a model considering the discrete behaviour of the liquids and powders. It also considered the slag and hot metal as two separate phases. Later, Nogami *et al.* [15] published another mathematical model of a blast furnace using the Bingham model, but no future study was carried out based on this model. In addition, Mondel *et al.* [16] published a mathematical model of a blast furnace considering the kinetic theory of the random motion of granular materials in a fluid flow. The dual nature of solid particles was also considered in this model. Furthermore, the concept of granular temperature [37] was adopted to describe this dual nature of solid particles. However, the focus of their study was on the profile of the raceway rather than the solid flow in the upper part of a blast furnace. Dong *et al.* [18] published their model based on Chen *et al.*'s [4] viscous model. In addition, the force balance method was used to calculate the liquid flow, in which the liquid (metal or slag) was treated as discrete droplets or rivulets. In 2010, Qing *et al.* [19] published a mathematical model of a blast furnace gas flow. In this article, the authors focused on the gas flow profile through the furnace with a designed layered structure.

It should also be mentioned that in addition to the above articles a couple of review papers can also be found. Yagi [3] is one of the pioneers who published a tremendous review article describing various aspect of the blast furnace mathematical modelling. Later on, Dong *et al.* [17] and Ueda *et al.* [20] also published review articles about the development of mathematical modelling of blast furnaces.

The overall information in **Table 1** illustrates that only Zhang *et al.* [8] considered the dual nature of the solid phase in the modelling of solid flow profile in the upper part of the blast furnace. Hence, since the focus of this study is on the movement of solid particles in the upper part of the furnace, it is crucial to include such phenomena to describe the behaviour of the solid particles in a packed bed.

Therefore, this investigation, which uses the previous study carried out by Zhang *et al.* [8] as a base, is intended to add information on the blast furnace process by modelling the solid particles behaviour considering the dual nature of this phase.

One of the important factors in any multiphase reactor, i.e. the blast furnace, is the porosity of the beds. Forsmo *et al.* conducted a study on the porosity of LKAB iron ore green pellets by packing in silica sand.[38] There are number of parameters affecting the particle packing such as the particle size and shape, surface texture, agglomeration, size distribution and container geometry.[39]

Based on the parameters mentioned above there is a limit with respect to the particle packing density. In theory, it is possible to have low packing densities with ordered packing of spheres. However, there are certain requirements such that the spheres should be in contact continually in a chain-like network to produce a structurally stable arrangement.[39] Of course (or may be 'it is known that'), the charging method and the porosity of the bed in a blast furnace can have a direct effect on the gas flow. Therefore, it can also affect the inter-granular forces between particles, due to the change in the packing of the bed. Hence, it is important to study and investigate the effect of the packing density on the profile of the solid phase in a blast furnace.

Table 1. List of selected articles about Mathematical modeling of the blast furnace

	Name	**Year**	**Review**	**Axi-symmetric**	**Inter-granular forces**	**Chemical Reaction**	**Dimension**		**Phases**			
							2D	**3D**	**Gas**	**Solid**	**Liquid**	**Powders / Fines**
[1]	Yagi [3]	1993	√	---	---	---	---	---	---	---	---	---
[2]	Chen *et al.*[4]	1993	---	---	---	---	√	---	√	√	---	---
[3]	Austin *et al.* [5]	1997	---	√	---	√	√	---	√	√	√	√
[4]	Austin *et al.* [6]	1997	---	√	---	√	√	---	√	√	√	√
[5]	Austin *et al.* [7]	1998	---	√	---	√	√	---	√	√	√	√
[6]	Zhang *et al.* [8]	1998	---	---	√	---	√	---	√	√	---	---
[7]	Takatani *et al.* [9]	1999	---	---	---	√	---	√	√	√	√	---
[8]	Castro *et al.* [10]	2000	---	√	---	√	√	---	√	√	√	√
[9]	Castro *et al.* [11]	2001	---	√	---	√	√	---	√	√	√	√
[10]	Castro *et al.* [12]	2002	---	√	---	√	---	√	√	√	√	√
[11]	Castro *et al.* [13]	2002	---	√	---	√	---	√	√	√	√	√
[12]	Zhang *et al.* [14]	2002	---	---	√	---	√	---	√	√	---	---
[13]	Nogami *et al.* [15]	2004	---	√	---	---	√	---	√	√	---	---
[14]	Mondal *et al.* [16]	2005	---	---	√	---	√	---	√	√	---	---
[15]	Dong *et al.* [17]	2007	√	---	---	---	---	---	---	---	---	---
[16]	Dong *et al.* [18]	2009	---	√	---	---	√	---	√	√	√	√
[17]	Qing *et al.* [19]	2010	---		---				√	√	---	---
[18]	Ueda *et al.* [20]	2010	√	---	---	---	---	---	---	---	---	---
[19]	Castro *et al.* [21]	2011	---	---	---	√	---	√	√	√	√	√

This study is based on a continuum model. A three-dimensional conservation equation for a multi-phase system has been solved numerically with the finite volume method. The existing phases are gas and solid.

Supplement 1 of this study presents and introduces the mathematical model used to describe solid particles behavior in an industrial scale blast furnace process. The geometry has been adopted from the blue print of SSAB´s blast furnace M4 located in Oxelösund, Sweden. It should also be mentioned that due to the nature of the solid particles, an extra term has been added to the Navier-Stokes equation to model the surface stress tensor to describe the particle-particle interactions due to collision and packing.

Supplement 2 of the current study investigates the effects of the packing density of the bed on the profile of the flow in the upper part of the blast furnace (down to the tuyeres level) for three different packing densities of 0.68, 0.71 and 0.74 while the other parameters in the model were kept fix.

2 Theory and Model Description

2.1 Governing Equations: General Conservation Equations

As it was mentioned earlier, one of the approaches in modeling a blast furnace process is to assume that all the phases in a blast furnace behave as a continues phase. Therefore, based on the above assumption, the blast furnace process can be modeled based on the continuum mechanics theory in an Eulerian frame of reference. In this study, two separate sets of Navier-Stokes equations are solved and linked together by interfacial forces. The general conservation equation in Eulerian frame of reference can be written as follows:

$$\frac{\partial(\varepsilon_i \rho_i \Phi_i)}{\partial t} + \nabla.(\varepsilon_i \rho_i \vec{u}_i \Phi_i) = \nabla.\left(\varepsilon_i \Gamma_{\Phi_i} \nabla \Phi_i\right) + S_{\Phi_i} \quad \text{..... 1}$$

where ε_i is the volume fraction, ρ_i is the density and $\vec{u}_i$ is the velocity vector for phase i. Moreover, the effective diffusive transfer coefficient, Γ_{Φ_i}, is represented in different ways due to the dependent variable being considered. For example, in the velocity field, it represents the dynamic viscosity of the phase considered, μ_i. However, in order to adjust the reality of a solid phase discontinuity, **Equation 1** must be extended, so that it can describe the behavior of this phase more accurately.

Zhang *et al.* [8], presented the following modified equations for the flow of solid particles in a blast furnace:

$$\frac{\partial \varepsilon_s}{\partial t} + \nabla.(\varepsilon_s \vec{u}_s) = 0 \quad \text{..... 2}$$

$$\frac{\partial(\varepsilon_s \rho_s \vec{u}_s)}{\partial t} + \nabla.(\varepsilon_s \rho_s \vec{u}_s \vec{u}_s) = \nabla.\tau_s + \varepsilon_s \rho_s \vec{g} \quad \text{..... 3}$$

where $\vec{g}$ is the gravitational acceleration vector. In fact, particles can either behave as a fluid media or act as a stagnant fluid, providing a resistance to particle movement. Therefore, the surface stress τ_s in **Equation 3** may be considered to consist of two parts [40-44]:

$$\tau_s = \tau_{rd} + \tau_{ri} \quad \text{..... 4}$$

where, as it is introduced by Zhang *et al.* [8], τ_{rd} is the rate-dependent part of the surface stress and τ_{ri} is the rate-independent part. The variable τ_{rd} originates from the particle-particle kinetic interaction due to collision. Moreover, τ_{ri} originates from particle-particle contact interaction due to packing, including normal contact and shear friction.

In this study, the three-dimensional framework of **Equations 2-4** for a system of two-phase gas-solid has been used which can be defined as follows:

For the solid phase:

$$\frac{\partial \varepsilon_{\mathrm{s}}}{\partial t} + \nabla.\left(\varepsilon_s \vec{\mathrm{u}}_{\mathrm{s}}\right) = 0 \quad \ldots\ldots 5$$

$$\frac{\partial (\varepsilon_s \rho_s \vec{\mathrm{u}}_{\mathrm{s}})}{\partial t} + \nabla.\left(\varepsilon_s \rho_s \vec{\mathrm{u}}_{\mathrm{s}} \vec{\mathrm{u}}_{\mathrm{s}}\right) = -\varepsilon_s \nabla p_s - \beta\left(\vec{\mathrm{u}}_{\mathrm{s}} - \vec{\mathrm{u}}_g\right) + \nabla.\tau_{rd} + \nabla.\tau_{ri} + \varepsilon_s \rho_s \vec{g} \quad \ldots\ldots 6$$

For the gas phase:

$$\frac{\partial \varepsilon_{\mathrm{g}}}{\partial t} + \nabla.\left(\varepsilon_g \vec{\mathrm{u}}_{\mathrm{g}}\right) = 0 \quad \ldots\ldots 7$$

$$\frac{\partial (\varepsilon_g \rho_g \vec{\mathrm{u}}_{\mathrm{g}})}{\partial t} + \nabla.\left(\varepsilon_g \rho_g \vec{\mathrm{u}}_g \vec{\mathrm{u}}_g\right) = -\varepsilon_g \nabla p_g - \beta\left(\vec{\mathrm{u}}_{\mathrm{g}} - \vec{\mathrm{u}}_s\right) + \nabla.\tau_g + \varepsilon_g \rho_g \vec{g} \quad \ldots\ldots 8$$

where,

$$\varepsilon_{\mathrm{g}} + \varepsilon_{\mathrm{s}} = 1 \quad \ldots\ldots 9$$

Equation 9 represents the relationship between the volume fractions of different phases that exist in the system. Since the voidage of a bed in a real blast furnace can vary, the volume fractions should be considered as unknown parameters. In **Equations 6** and **8**, the parameter β represents the momentum transfer coefficient and is dependent on the gas volume fraction. For $\varepsilon_{\mathrm{g}} \leq 0.8$ then β should be evaluated based on the classical Ergun equation.[45] On the other hand, for $\varepsilon_{\mathrm{g}} > 0.8$ Richardson and Zaki's formulation should be used [46]. Hence, β could be represented as:

$$\beta = \begin{cases} 150 \frac{\varepsilon_s^2}{\varepsilon_{\mathrm{g}}} \frac{\mu_{\mathrm{g}}}{\left(\varphi_s d_{\mathrm{p}}\right)^2} + 1.75\, \varepsilon_{\mathrm{s}} \frac{\rho_{\mathrm{g}}}{\varphi_s d_{\mathrm{p}}} \left|\vec{\mathrm{u}}_{\mathrm{g}} - \vec{\mathrm{u}}_s\right| & \varepsilon_{\mathrm{g}} \leq 0.8 \\ \frac{3}{4} C_d \frac{\varepsilon_g^{-1.65} \varepsilon_{\mathrm{s}}}{\varphi_s d_{\mathrm{p}}} \rho_{\mathrm{g}} \left|\vec{\mathrm{u}}_{\mathrm{g}} - \vec{\mathrm{u}}_s\right| & \varepsilon_{\mathrm{g}} > 0.8 \end{cases} \quad \ldots\ldots 10$$

where the parameter φ_{s} represents the sphericity of the particle, $\mathrm{d_p}$ is the diameter and $\mathrm{C_d}$ is the drag coefficient and is related to the particle Reynolds number $\mathrm{Re_p}$ as follows:

$$C_d = \begin{cases} \frac{24}{\mathrm{Re_p}} \left[1 + 0.15\, Re_p^{0.687}\right] & \mathrm{Re_p} \leq 1000 \\ 0.44 & \mathrm{Re_p} > 1000 \end{cases} \quad \ldots\ldots 11$$

The particle Reynolds number in **Equation 11** is defined in the following manner:

$$Re_p = \frac{\varepsilon_{\mathrm{g}} \rho_{\mathrm{g}} \left|\vec{\mathrm{u}}_{\mathrm{g}} - \vec{\mathrm{u}}_s\right| d_{\mathrm{p}}}{\mu_{\mathrm{g}}} \quad \ldots\ldots 12$$

2.2 Governing Constitutive Equations: Surface Stress

To be able to fully describe the above equations, it is necessary to determine the constitutive equations. The constitutive equations need to be presented for both phases, i.e. gas and solid, in the system. In addition, other related parameters like the solid viscosity, elastic modulus and friction coefficient should be determined. The constitutive equation for the gas phase is referred to as the viscous stress and it can be expressed as:

$$\tau_g = 2\varepsilon_{\mathrm{g}} \mu_{\mathrm{g}} D_{\mathrm{g}} - \frac{2}{3} \varepsilon_{\mathrm{g}} \mu_{\mathrm{g}} tr D_{\mathrm{g}} I \quad \ldots\ldots 13$$

where μ_{g} is the gas viscosity, $\mathrm{D_g}$ is gas stretching tensor, trD_{g} is the trace of the stretching tensor and I is the identity matrix. This equation is based on the Newtonian expression.

As already stated, the solid surface stress consists of a rate-dependent and a rate-independent part. The rate-dependent part, similarly to the gas viscous stress equation, is the Newtonian part of the

constitutive equation for the solid phase. Therefore, the viscous part of the solid surface stress equation is expressed as:

$$\tau_{rd} = 2\varepsilon_s\mu_s D_s - \frac{2}{3}\varepsilon_s\mu_s trD_s I \quad \text{..... 14}$$

where μ_s is the solid viscosity and D_s is solid stretching tensor associated with the motion of particles. The rate-independent part of the solid surface equation is based on the Coulomb frictional relation and can be expressed as follows:

$$\tau_{ri} = -P_e I + 2\eta_s \frac{D_s}{\sqrt{trD_s^2}} \quad \text{..... 15}$$

where P_e is the effective pressure and η_s is the coefficient of plastic modulus. The variable η_s is based on Norem *et al.* [47]:

$$\eta_s = \frac{1}{\sqrt{2}}(\alpha_1 + \alpha_2 P_e^n) \quad \text{..... 16}$$

where α_1 is equal to zero for cohesionless materials and n is equal to 1 corresponding to the Coulomb frictional model. In addition, the friction coefficient α_2 can be expressed as follow:

$$\alpha_2 = \frac{\left|\frac{\partial w_s}{\partial x}\frac{1}{w_s}\right|}{\left|\frac{\partial w_s}{\partial x}\frac{1}{w_s}\right|_{Max}} \tan\phi \quad \text{..... 17}$$

where w_s is the components of the velocity vector for solid phase in z-direction, ϕ is the internal friction angle and Max is the maximum value in the flow field domain.

The effective pressure P_e, in **Equations 15** and **16** is reported by Zhang *et al.* [8] as follows and is employed according to the normal component of the surface stress due to Orr [48]:

$$P_e = \frac{G_0}{c} e^{c(\varepsilon_s - \varepsilon_s^*)} \quad \text{..... 18}$$

where G_0 is the normalizing unit factor, c is the compaction modulus and ε_s^* is the packing density, i.e. the solid volume fraction measured under the standard loose or poured packing condition. The parameters G_0 and c are constants and are reported by Zhang *et al.* [8] as 1.0 Pa and 150 respectively.

2.3 Source Term

The source term S_{Φ_i} in **Equation 1** is due to external forces such as body forces, which arise through gravitational forces. Furthermore, $S_{\Phi_i}$is also due to inter-phase interactions which arise through chemical reactions [5-7, 9] or surface interactions. Chen *et al.* [4] included the friction force between particles and walls or the deadman to the source term in addition to the body force. These surface interactions can be due to the effect of gas on solid particles, which is formulated based on Ergun's equation [45] and Richardson and Zaki.[46] Moreover, S_{Φ_i}also includes solid-solid friction-collision which is described by constitutive equations.[8] In this study, the source term is based on the body force, the effect of gas on solid particles, and particle-particle interaction.

2.4 Initial and Boundary Conditions

To solve any differential equation it is necessary and critical to specify appropriate boundary conditions. In fact, when a differential equation is to be solved, the solution would be highly dependent to the boundary conditions defined in the domain. Therefore, to be able to find a solution for **Equations 5-8**, appropriate boundary conditions for the blast furnace process have to be identified and introduced to the solver.

In a blast furnace process simulation, the essential boundary conditions are actual furnace operational conditions. For example, the velocity of gas at the tuyeres, the top gas pressure, the solid mass flow at

the top of the furnace which is called throat and the removal rate of solid particles at the bottom of the domain. Moreover, a blast furnace flow is a counter-current flow which means that the existing phases in the system travel in opposite directions. Therefore, the top layer acts as an inlet for the solid phase while it serves as an outlet for the gas. The solid outlet is located at the bottom of the domain so that the solid particles could leave the domain from the bottom. In summary, the following boundary conditions have been used in this study:

- A pressure boundary is used at the top of the domain to remove the gas.
- Solid particles are assumed to be charged homogeneously at the top of the domain with a velocity giving a mass flow rate of 90 kg/s.
- A solid velocity is set at the solid outlet based on the mass flow rate of the solid phase at the top.

The deadman in a blast furnace plays an important role. Therefore, the information on the characteristics of the deadman in any blast furnaces modeling is essential. In most of the blast furnace modelling, the characteristics of the deadman are set in the model. However, Zhang *et. al.* [8] presented a method to define the boundary of the deadman based on the velocity of the solid phase in the system. Nevertheless, the method described in their study only considers the velocity of the particles. In this study, the characteristics of the deadman e.g. shape, size and height are set based on a field study during a relining which was done on the SSAB blast furnace in Oxelösund, Sweden.[49]

The no-slip boundary condition cannot be applied at the impenetrable solid wall.[50, 51] In fact, partial slip of solids at the wall is possible. Therefore, the solid tangential velocity, u_{s_z}, at the wall is assumed to be proportional to its gradient at the wall. This is due to the fact that the particle diameter is usually larger than the length scale of the surface roughness of the rigid wall. Therefore, the solid tangential velocity at the wall can be expressed by [8]:

$$w_s|_{wall} = -\lambda_p \frac{\partial w_s}{\partial x}|_{wall} \quad \text{..... (19)}$$

where w_s is the solid velocity in z-direction, x is the normal direction to the wall and the slip parameter λ_p can be described by [50, 51]:

$$\lambda_p = \frac{1}{\varepsilon_s^{1/3}} d_p \quad \text{..... (20)}$$

The λ_p denotes the mean distance between particles. This equation shows that for small particles, the boundary condition is close to the no-slip condition.

As for the initial conditions, the important factor is the volume fraction of phases considered in the model. Since there are two physical phases present in this model, i.e. solid and gas, the ratio between these phases must be initially set according to the reality of the model by using **Equation 9**.

The current model is a two-phase model of the gas-solid movements in the upper part of the blast furnace. However, to further simplify the model in this study, the velocity of the gas at the tuyers level is assumed to be zero. However, a back flow for gas is permitted at the solid outlet so that the material balance would be fulfilled. Note that even though the gas velocity is set to zero; the equations have been solved for the volume fraction to calculate the voidage of the bed in the furnace.

2.5 Geometry and Mesh Structure

In this study, the simulations have been done for an industrial blast furnace. The geometry has been made based on the blue print of M4 blast furnace of SSAB, located in Oxelösund, Sweden. **Figure 1** shows the geometry and size of the furnace. The calculation has been done on a quarter of the furnace. The diameter of the belly is equal to 10.6 m and its height is equal to 20.0 m.

As seen in **Figure 1** the constructed domain is only from the tuyeres level up to the throat, since the focus of this study is on the solid flow profile in the upper part of the furnace. The coordinate origin is located at the bottom-left corner of the domain. The cut-cell method was used to construct the mesh. **Figure 2.1** shows the mesh structure for the furnace geometry. The simulation mesh can be seen in **Figure 2.2**. The grid dimension was [53×53×100], respectively.

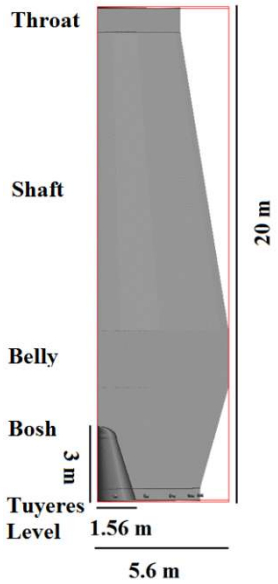

Figure 1 The size and shape of the SSAB M4 blast furnace.

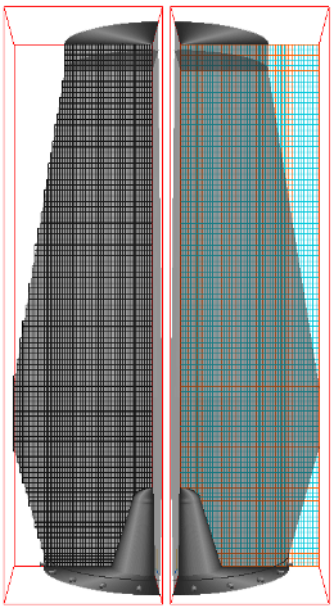

Figure 2.1 Constructed mesh for the furnace geometry: left
2.2 Constructed mesh for the domain of calculation: right

In the current model, commercial CFD code PHOENICS was used to solve a two-phase, three-dimensional flow. A staggered grid was employed with the differencing scheme SMART [52] to solve the partial differential equations by converting it to algebraic finite volume equations. The equations are solved iteratively using the IPSA algorithms.[53]

Intentionally left blank!

3 Results

The results are presented in three sections. In the first section, the solid phase velocity for different heights is plotted to show the behavior of solid phase as it descends through the blast furnace. Next, a comparison is made between three cases: i) one case without the extra term in Navier-Stokes equations represented by **Equations 14-18**, the other two with the extra term in Navier-Stokes equation included and the compaction modulus set to ii) 150.0 and iii) 230.0, respectively. Finally, the effect of a changed solid volume fraction on the profile of the solid phase is presented. **Figure 3** shows the position and distance of each grid-slab being studied.

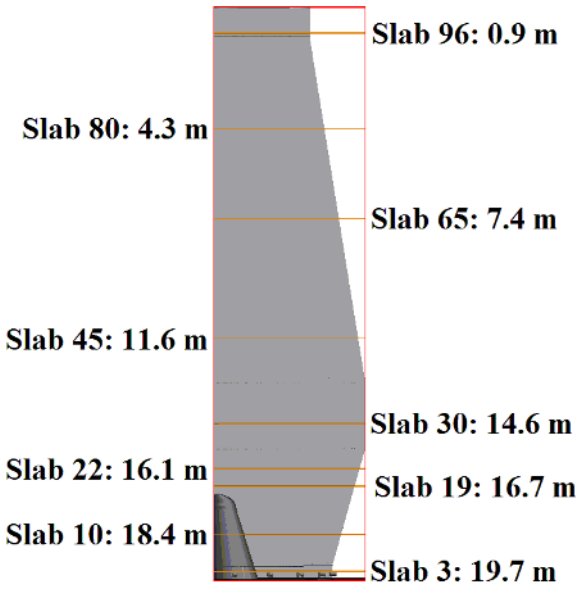

Figure 3 The chosen slabs and their distance from the top.

3.1 Velocity profile at different heights

Figures 4.1-4 show the velocity profiles for slabs 96, 80, 65 and 45, which are located in the upper part of the furnace. For these slabs, it can be seen that the maximum velocity can be found along the center axis which is reduced from slab 96 to 45. The magnitude of velocity at the center axis for slab 96 is around 0.87 mm/s, while this magnitude is 0.41 mm/s in slab 45 (11.6 m below the top).

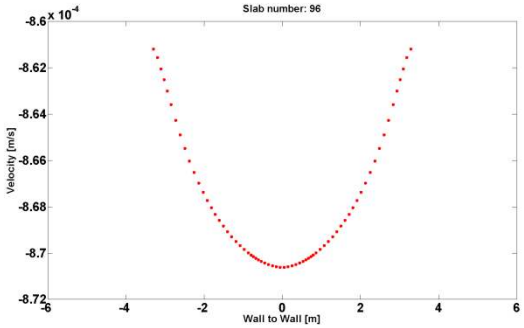

Figure 4.1 Velocity profile for slab 96: $(8.6{,}8.72)\times10^{-4}$ [m/s]

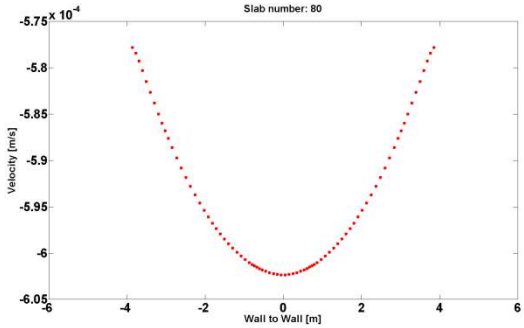

Figure 4.2 Velocity profile for slab 80: $(5.75{,}6.05)\times10^{-4}$ [m/s]

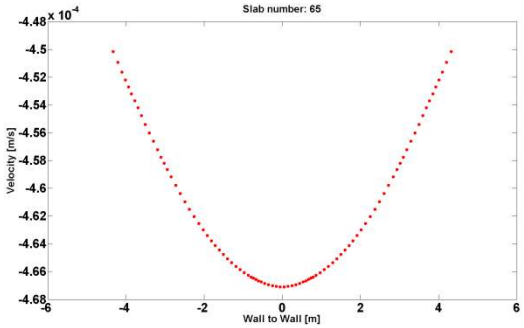

Figure 4.3 Velocity profile for slab 65: $(4.48, 4.68)\times10^{-4}$ [m/s]

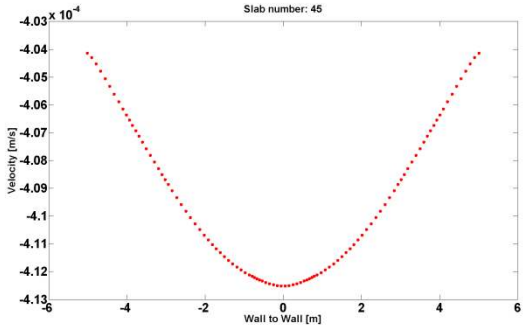

Figure 4.4 Velocity profile for slab 45: $(4.03, 4.13)\times10^{-4}$ [m/s]

Figure 4.5 shows the velocity profile at the belly of the furnace. It can be seen that the velocity profile around the center axis changes its shape and flattens out. It can also be seen that the velocity profile close to the furnace wall changes its shape in comparison to what was seen in the upper slabs. **Figure 4.6** shows the velocity profile for the solid phase at slab 22. This slab is located 1.6 m above the deadman. This figure shows that the solid phase profile changes its shape and that the maximum velocity magnitude appears at the sides, where the outlet is located.

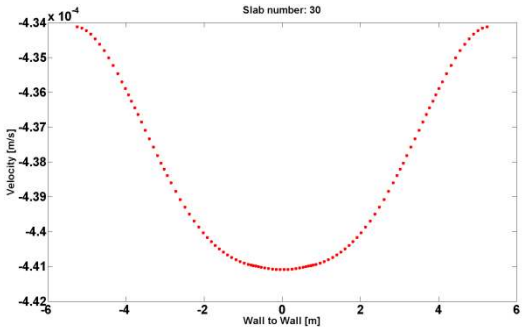

Figure 4.5 Velocity profile for slab 30: $(4.34, 4.42)\times10^{-4}$ [m/s]

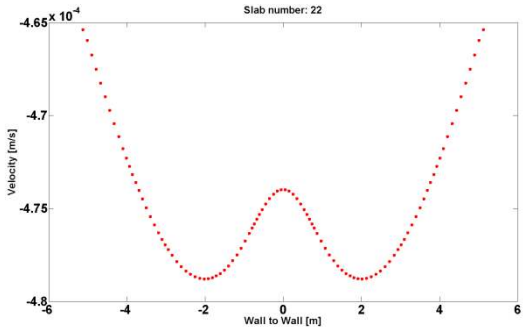

Figure 4.6 Velocity profile for slab 22: $(4.65, 4.80)\times10^{-4}$ [m/s]

The velocity profile for slab 19, which is located 16.7 m below the top in **Figure 4.7**, shows the same behavior. Moreover, it is shown that the magnitude of the velocity at the center axis is even lower than at the wall-neighboring cells. It should also be mentioned that the velocity magnitude increases at slab 22 in comparison to slab 30. This increase in the magnitude of the velocity can be seen for all the slabs below the belly. Slab number 10 is located below the top of the deadman. Therefore, the velocity profiles are divided to two separate sections. At this slab, the magnitude of velocity for the cells close to the deadman boundary is larger than at the wall-neighboring cells. However, this behavior is reversed at slab number 3, which is located 0.4 m above the outlet. At this slab, the magnitude of the velocity for wall-neighboring cells are higher than for those cells located close to the deadman boundary.

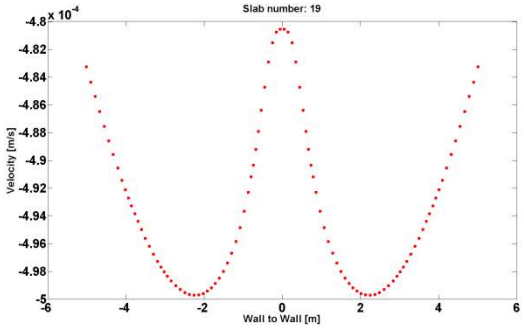

Figure 4.7 Velocity profile for slab 19: $(4.8, 5.0)\times10^{-4}$ [m/s]

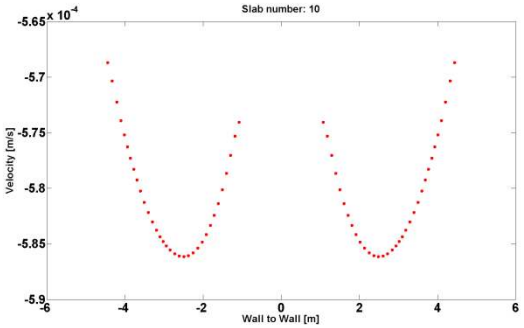

Figure 4.8 Velocity profile for slab 10: $(5.65, 5.90)\times10^{-4}$ [m/s]

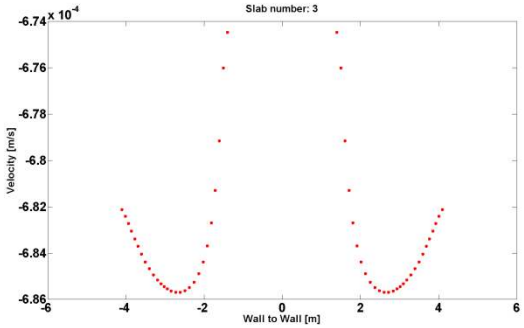

Figure 4.9 Velocity profile for slab 3: $(6.74, 6.86)\times10^{-4}$ [m/s]

3.2 Comparison of velocity profiles

As mentioned above, the results from three different cases have been studied: i) one case without the extra term in Navier-Stocks equations represented by **Equations 14-18** and two cases with these terms included and with compaction modulus c equal to ii) 150.0 and iii) 230.0 in **Equation 18**, respectively. The results are shown in **Figures 5.1-9**.

Figure 5.1 shows the velocity profiles at slab number 96. The dotted line represents the case without the extra term. The dashed and solid lines show the cases for c equal to 150.0 and 230.0, respectively.

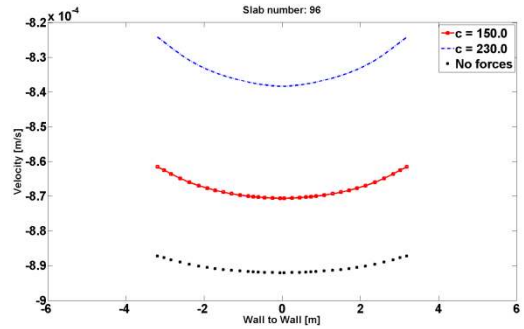

Figure 5.1 Solid phase velocity for slab 96 wrt P_e: $(8.2, 9.0)\times10^{-4}$

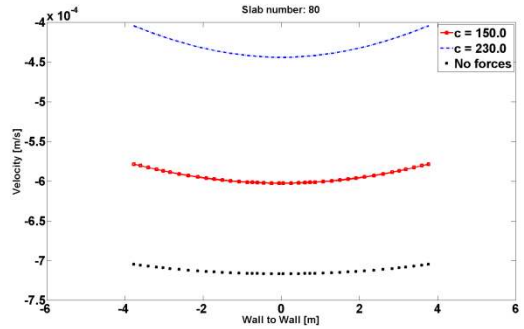

Figure 5.2 Solid phase velocity for slab 80 wrt P_e: $(4.0, 7.5)\times10^{-4}$

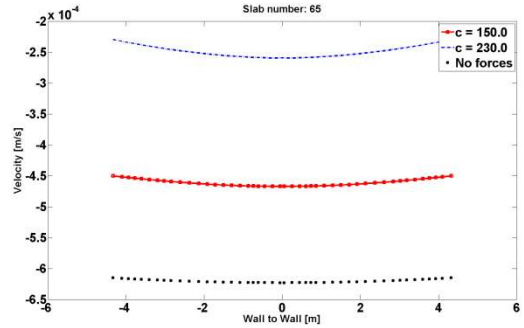

Figure 5.3 Solid phase velocity for slab 65 wrt P_e: $(2.0,6.5)\times10^{-4}$

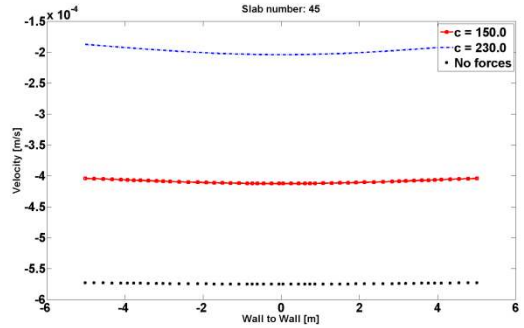

Figure 5.4 Solid phase velocity for slab 45 wrt P_e: $(1.5,6.0)\times10^{-4}$

Figure 5.1 shows that the case without forces has the highest velocity magnitude. Moreover, that the case with the highest value of c (equal to 230.0) has the lowest magnitude of the velocity. Also, noted is that the magnitude of the difference between the first and second case is less than the differences in magnitude of the velocity from second and third case. The same behavior can be seen for all the other slabs at the lower level of the blast furnace. The same comparisons of the velocity magnitude in **Figures 5.5-6** shows that the case with a c value equal to 230.0 has a deeper curvature than the case with a c value equal to 150.0. In addition, the velocity profiles for case without forces almost represent a flat line in slab 30 as illustrated in **Figure 5.5**.

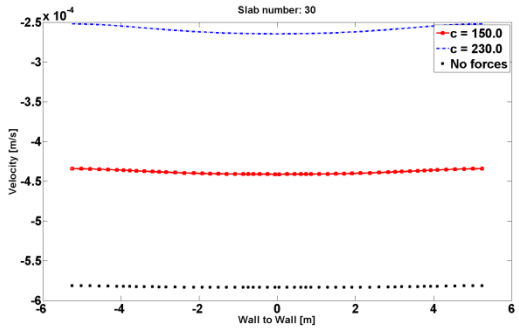

Figure 5.5 Solid phase velocity for slab 30 wrt P_e: $(2.5,6.0)\times10^{-4}$

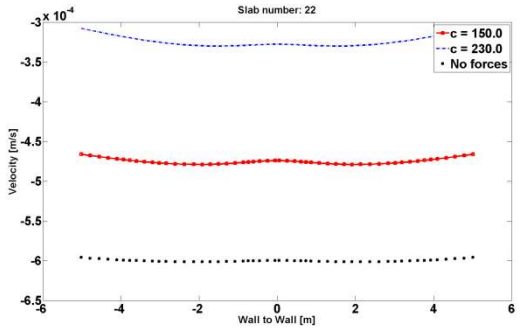

Figure 5.6 Solid phase velocity for slab 22 wrt P_e: $(3.0,6.5)\times10^{-4}$

Moreover, the velocity profile for a c value equal to 230.0 in **Figure 5.6** shows a stronger effect with respect to the boundary of the deadman. The same behavior can also be seen at slabs 19, 10 and 3.

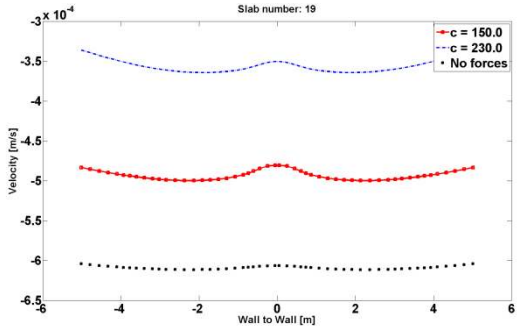

Figure 5.7 Solid phase velocity for slab 10 wrt P_e: $(3.0,6.5)\times10^{-4}$

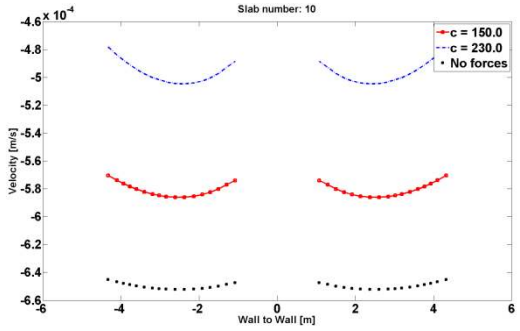

Figure 5.8 Solid phase velocity for slab 10 wrt P_e: $(4.6,6.6)\times10^{-4}$

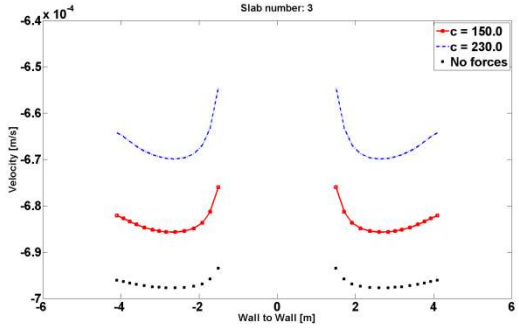

Figure 5.9 Solid phase velocity for slab 3 wrt P_e: $(6.4, 7.0)\times10^{-4}$

3.3 Effects of the solid volume fraction on the profile of the solid phase

The solid phase velocity profiles have been studied and evaluated for different heights in the furnace, as shown in **Figure 3**. **Figures 6.1-9** show the velocity profile of the solid phase at different heights for three cases with solid volume fractions equal to 0.68, 0.71 and 0.74, respectively. As seen, the velocity profiles follow the same behavior from the top to the bottom of the furnace.

For slabs 96, 80, 65 and 45, the maximum value for the solid velocity appears at the center axis. **Figure 6.1** shows the velocity profiles for the solid phase at slab 96 for different solid volume fractions. This slab is located 0.9m below the top surface of the domain. It can be seen that the velocity magnitude is reduced by an increment in the volume fraction of the solid phase. Of course, an increase in the volume fraction of the solid phase reduces the porosity of the beds. Therefore, the particles have less space to slide into, which increases the solid-solid particles contact.

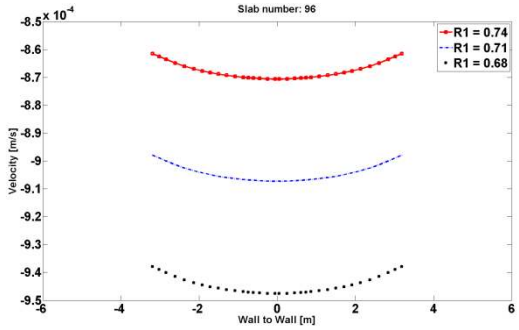

Figure 6.1 Velocity profile for slab 96 wrt solid volume fraction: $(8.5, 9.5)\times10^{-4}$ [m/s]

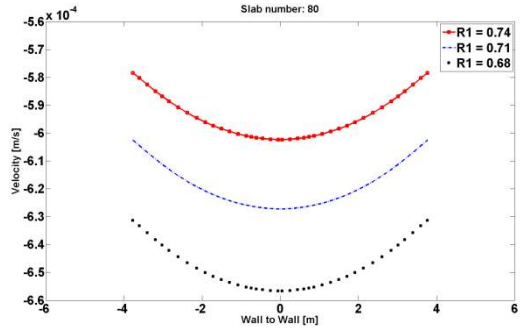

Figure 6.2 Velocity profile for slab 80 wrt solid volume fraction: $(5.6, 6.6)\times10^{-4}$ [m/s]

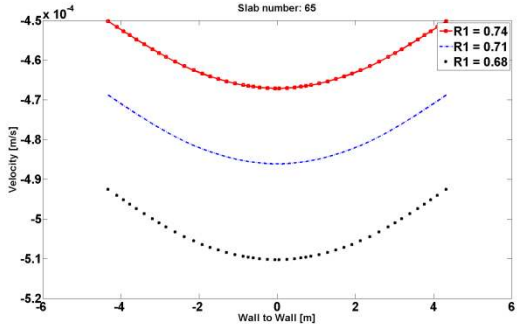

Figure 6.3 Velocity profile for slab 65 wrt solid volume fraction: $(4.5, 5.2)\times10^{-4}$ [m/s]

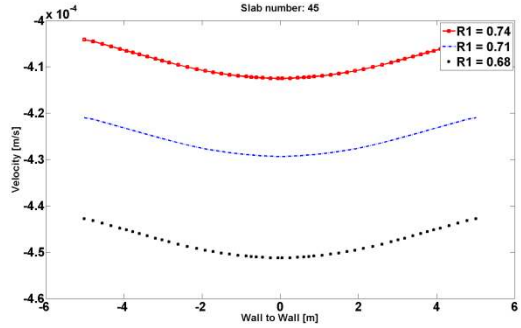

Figure 6.4 Velocity profile for slab 45 wrt solid volume fraction: $(4.0, 4.6)\times10^{-4}$ [m/s]

It has been shown that the solid-solid contact forces act as a break and resist the descending movements of the solid particles. Therefore, an increase in the volume fraction of the solid phase decreases the magnitude of the solid phase velocity, which is shown in **Figure 6.1**. The same behavior can be seen for the slabs located below slab 96. Moreover, the magnitude of the difference between the cases with volume fractions values equal to 0.68 and 0.71 is equal to a value of 4.0×10^{-5}. However, for the cases with volume fraction values equal to 0.71 and 0.74 this difference is equal to a value of 3.6×10^{-5}. It shows that the decrease in the magnitude of the velocity is slightly lower between cases 0.71 and 0.74 in comparison to cases 0.68 and 0.71. The same values for slab 80 are 2.9×10^{-5} and 2.4×10^{-5}, respectively. Therefore, it can be said that the magnitudes of the differences decrease between two following slabs from slab 96 to 80 down to slab number 45. However, the differences start to increases at slab 30 and this increase continues down to slab number 3.

Moreover, the maximum value of solid phase velocity for slab 30 is also positioned at the center axis. However, at this slab the velocity profile for all three cases is flattened out around the center axis. Furthermore, the maximum velocity value at slab 22 positioned just above the deadman (see **Figure 3**) is shifted to the side due to the central position of the deadman. Of course, the position of the maximum velocity value is also due to the shape and position of the outlet, which is located at the bottom of the domain. The solid outlet located at the bottom of the furnace has a ring-like shape surrounding the deadman.

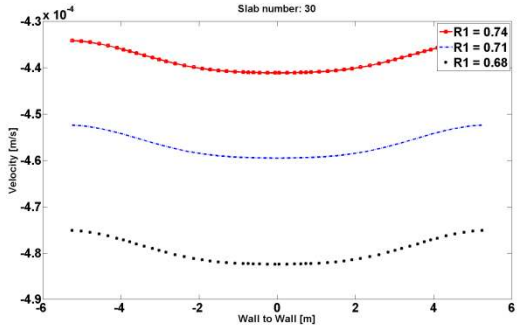

Figure 6.5 Velocity profile for slab 30 wrt solid volume fraction: $(4.3,4.9)\times10^{-4}$ [m/s]

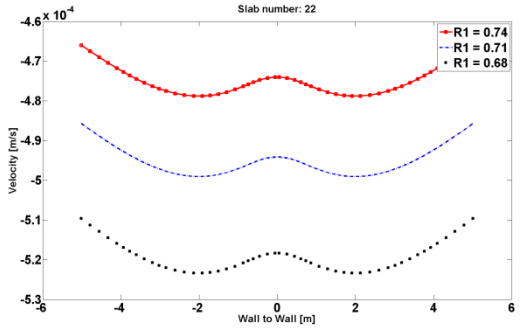

Figure 6.6 Velocity profile for slab 22 wrt solid volume fraction: $(4.6,5.3)\times10^{-4}$ [m/s]

Therefore, the particles have to move to the side from the center axis so that they can leave the domain. Slab 19 shows the same behavior, but the solid profile has a deeper curvature in comparison to the solid profile at slab 22 due to the location of this slab and its distance to the top of the deadman. Slab 19 is located 0.3m above the deadman (see **Figure 3**). Due to the profile of the deadman it is also seen that the solid profiles for slabs 10 and 3 are disconnected (**Figures 6.8** and **6.9**).

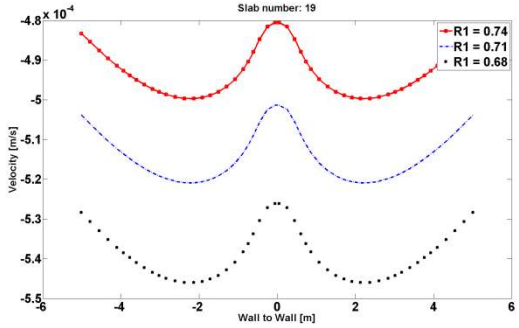

Figure 6.7 Velocity profile for slab 19 wrt solid volume fraction: $(4.8,5.5)\times10^{-4}$ [m/s]

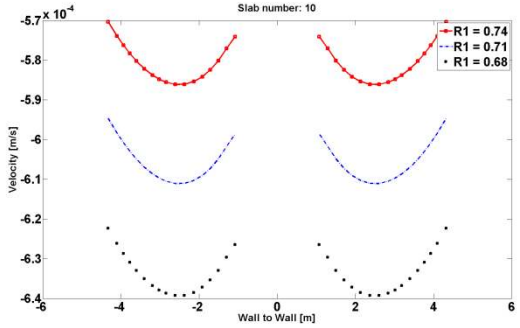

Figure 6.8 Velocity profile for slab 10 wrt solid volume fraction: $(5.7,6.4)\times10^{-4}$ [m/s]

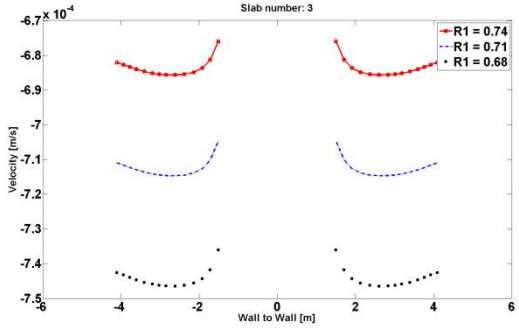

Figure 6.9 Velocity profile for slab 3 wrt solid volume fraction: $(6.7,7.5)\times10^{-4}$ [m/s]

Of course, it is of a great interest to study the difference in the velocity profiles to have an overall view of the changes in the solid flow in a blast furnace. **Figure 7** shows the maximum velocity for the different solid volume fractions 0.68, 0.71 and 0.74, respectively.

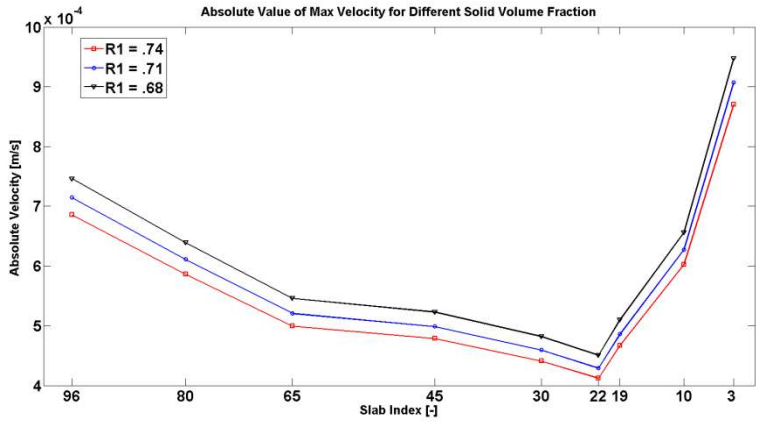

Figure 7 Absolute value of maximum velocity for solid volume fraction equal to 0.74, 0.71 and 0.68 at different slabs

As can be seen, the slope between two following slabs is almost the same for the different cases for a charged solid volume fraction. In other word, these three different cases are parallel in every section. This indicates that the solid phase behave in similar manner for different charging procedures with respect to the magnitude of the maximum velocity. Moreover, the angle of the slope between slab 96 and slab 80 is larger than the angle of the slope for slabs 80 to 65. Furthermore, the angle of the slope for slabs 80 to 65 is almost equal to that for slabs 65 to 45. However, the slope changes its sign at slab 45, which indicates that the magnitude of the velocity increases from this slab. This change can be seen for all three cases of a charged solid volume fraction. In addition, the angle of the slope between slabs 45, 30, 22 and 19 is almost similar whereas the angle of the slope increases rapidly after slab 19. However, a small change in the angle of the slope can be seen between slabs 22 to 19 in comparison to the data presented in the previous section.

Figure 8 shows the maximum velocity for different slabs with respect to the charged solid volume fraction. It is important to note that all the lines in **Figure 8** have almost identical slopes. This indicates that the changes in the magnitude of the maximum velocity for different solid volume fractions at all the slabs are equal. The solid lines in **Figure 8** show the changes for slabs 96, 80 and 65 which shows a steep decrease from the throat towards the belly is seen. Furthermore, dashed lines show changes in the maximum velocity for slabs 45, 30 and 22 over the belly. In contrast, the change in maximum velocity is not very significant in this area. However, the dotted lines, which represent slabs 19, 10 and 3, show a quite steep change below the belly region.

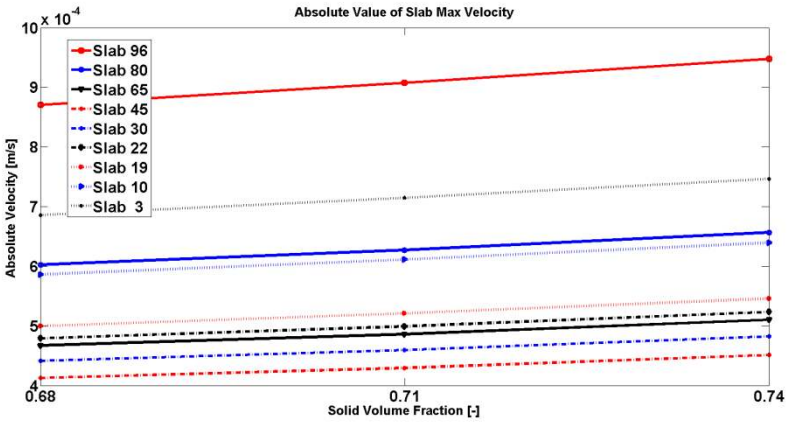

Figure 8 Absolute value of maximum velocity at different slabs wrt solid volume fraction

Intentional left blank!

4 Discussion

Below the results are discussed. Thereafter, a comparative study has been done between results presented in Zhang *et al.* [8] article and the results for the case of a solid volume fraction equal to 0.68 in the current study. Note, that in the current study an operational full scale blast furnace was the focus of investigation while Zhang *et al.* [8] used a small laboratory scaled furnace.

As explained in the previous section, the maximum velocity for slabs 96, 80, 65 and 45, which are shown in **Figures 4.1-4**, appear at the center axis of the domain. This shows that the solid phase up to the belly of the furnace behave more like a pipe flow. Also, noted is that the velocity magnitude is reduced in this region with lower heights (from slab 96 towards 45). Moreover, based on the simulated mass flow rate the inlet velocity at the top of the furnace is set as a constant value normal to the throat face. Therefore, an increase in the magnitude of the area of any horizontal grid-slab reduces the magnitude of the velocity. This is due to that the velocity has an inverse relation to the area of the cross section in the calculation of the mass flow. However, **Figure 4.5** showed that for slab number 30 the velocity at the center axis is flattened out and does not have a sharp edge at this axis. This shows the effect of the deadman boundary on the velocity profile. In other words, the solid particles are reducing their velocity at the center axis due to the fact that there is a blockage area at the middle of the domain. In **Figure 4.6**, this can also easily be seen on the profile of the velocity for slab 22. It is seen that the maximum velocity value is shifted from the center line towards the side, above the location of the outlet. **Figure 4.7** shows a similar behavior with a higher magnitude of effect for slab 19. In fact, the center axis velocity at this slab is even lower than the magnitude of the velocity of the solid phase close to the furnace wall due to the location of the deadman at the middle-bottom of the furnace. **Figures 4.8** and **4.9** show the velocity profile of the solid phase at slabs 10 and 3. As seen, the velocity profiles for these two slabs are divided into two different disconnected parts. This is of course due to the size and height of the deadman. **Figure 4.8** shows that at slab number 10, the velocity of the solid phase close to the boundary of the deadman is higher in magnitude than it is in the wall neighboring cells at the same slab. This can be due to the shape of the domain at this slab, which shows that the deadman boundary has a lower angle than the furnace wall. On the other hand, **Figure 4.9** shows the opposite effect. The solid phase has a higher velocity at the wall neighboring cells than the deadman boundary cells at slab number 3. This can be due to the location of the slab. As it can be seen in **Figure 3** slab number 3 is located at the tuyeres level of the furnace geometry. At the outer face it has a cylindrical shape while at the deadman boundary face it follows the slope of the deadman. Therefore, the changes in the magnitude of the velocity for wall neighboring and the deadman boundary cells can be due to the geometry of the domain at this level as well.

Figure 5.1-9 show the velocity profile for the solid phase for three different cases: i) without forces, ii) with forces and for a compaction modulus equal to 150.0 and iii) with forces and for a compaction modulus 230.0. **Figure 5.1** shows the velocity profiles for these three cases. The velocity magnitude is

higher for the first case (without forces) than for the case with a compaction modulus equal to 150.0. This means the extra terms in the Navier-Stocks equation defined by **Equations 14-18** behave as a breaking force. Of course, due to the shape and characteristic of beds in a blast furnace, particles are in contact with their neighboring particles which prevent particles from sliding through. In other words, it can be said that this contact force behaves like a friction force and counteracts the vertical velocity. This behavior can be seen in **Figure 5.1** which shows that **Equations 14-18** simulate the particle-particle contact forces. In addition, **Figure 5.1** also shows the effect of an increased magnitude of the compaction modulus on the velocity profile of the solid phase. In fact, an increased magnitude of the compaction modulus reduces the velocity profile magnitude. This means that the interaction forces between particles increases when the value of the compaction modulus increases. It should also be mentioned that the case with a larger compaction modulus has a deeper curvature than the other two cases. The case with compaction modulus equal to 230.0 has a deeper curvature than the case with a compaction modulus equal to 150.0. Moreover, the same trend can be seen between the case with the compaction modulus of 150.0 and the case with no forces. This means that the difference between the minimum and maximum of velocity profile for the case with a compaction modulus 230.0 is higher than for the other cases. **Figures 5.2-9** also show this behavior. A stronger effect of this curvature behavior can be seen in **Figure 5.5** (slab number 30). The velocity profile for the case with no forces looks almost like a flat line. However, for the case with a compaction modulus of 230.0 some curvature can be identified. This is even more clear for slabs 22 and 19. The same trend with larger effect can also be seen for slabs 10 and 3.

Figure 6.1 shows that the magnitude of the velocity increases while the solid volume fractions are reduced at slab 96 at the top of the furnace. Since the boundary condition at the top of the furnace is set based on the mass flow rate, the reduction of the solid volume fraction at the constant surface area will result in an increment of the magnitude of the velocity for the solid particles. In fact, a reduction in the solid volume fraction magnitude leads to an increase in the porosity of the surface area. The increase in the porosity of the surface area not only means less packing, but also makes it easier for solid particles to slide through and to cause fewer collisions. Therefore, the increase in the porosity of the surface area increases the velocity magnitude. This behavior is also shown in **Figures 7** and **8**. **Figure 6.1** shows that the magnitude of the velocity for the case with a porosity value equal to 0.32 is slightly less than 9.5×10^{-4} m/s, while it is almost 8.7×10^{-4} m/s for the case with a porosity value equal to 0.26. On the other hand, the increase in the surface area and volume fraction occurring from slab 96 to 80 leads to a reduction in the magnitude of the velocity. Since chemical reactions are not considered, the mass flow rate at each slab is constant. Therefore, an increase in the surface area of the solid volume fraction will result in a decrement of magnitude of the velocity. The same behavior can be seen for slabs 65, 45 and 30, since the surface area increases from the throat up to the belly of the furnace. However, at slab 30 the velocity profile is flattened at the center axis. This is due to the location and shape of the deadman. Of course, the particles cannot leave the domain from the middle of the domain at the bottom, since it is blocked by the deadman. Therefore, their velocity is reduced at the center axis. However, the behavior of the velocity profile for the three different cases of volume fractions mentioned earlier still remains. At slab 22 and 19, the velocity magnitude is further reduced at the center axis since the particles are affected by the deadman shape. Moreover, **Figure 7** shows that the angle of slope between slabs 22 to 19 is slightly higher than for the previous slabs. This should be due to the decreased area since slabs 22 and 19 are located below the belly of the furnace. Furthermore, a large area of the furnace at the bottom is also blocked by the deadman. This reduces the effective area further, so the particles face the blocking at the lower level which leads to a larger decrease in the velocity magnitude. This manifests itself as a lower angle of the slope in **Figure 7**. However, the velocity profile for slabs 10 and 3 is disconnected at the middle due to the location of the deadman. Since the deadman height is larger than the height of these two slabs, there is no particle movements at the middle of these slabs. It could be noted that the shape of the velocity profiles behave in a similar manner from slab 96 (at top of the domain) down to slab 3 (above the outlet at the tuyeres level).

The data in **Figure 7** also support the above conclusion. As seen, the maximum velocity drops at the first part and after the belly (slab 30) it starts to increase. Furthermore, the difference in the angle of

the slope specifies the increase/decrease of the velocity from one slab to the other. As can be seen, the angle of the slope is the same between slabs 96-80 to 80-65. This means that the decrease in the magnitude of velocity is the same for these slabs. However, the angle is changing for slab 65-45 which identifies that the decrease in the velocity magnitude from slab 65 to 45 is not as large as in previous part of the furnace. Meanwhile, there is a sudden change in the direction of the slopes after slab 22, which represents the increase in the magnitude of the velocity. This is also verified by the data presented in **Figures 6.1-9**. Moreover, the angle of the slope is larger for slab 10-3 in comparison to slab 19-10. This explains why the velocity magnitude increases more from slab 10 to 3 than from slab 19 to 10.

It should be noted that the particle size shrinkage is not considered in the current model. Therefore, it is hard to derive a general conclusion with respect to a production furnace. It is also known that the shrinkage appears at the lower part of the furnace. Hence, it is plausible that a decrease in the porosity of the bed leads to an increased descending time of the particles. Of course, an increase in the descending time means a longer gas-solid contact. This, in turn, can lead to an increase of the gas-solid reaction as well as diffusion of the gas into the solid particles.

As mentioned earlier, this study is based on a previously published work by Zhang *et al.*[8] However, in that study a laboratory scale furnace was used. In the current study the geometry is based on a full scale operational blast furnace, which is located at SSAB, in Oxelösund, Sweden. Therefore, a comparison seems relevant between these two studies. Below, the domain of calculation is compared first, followed by comparing the velocity fields between these two studies.

Table 2 shows a comparison between the two geometry parameters. Moreover, as can be seen in Zhang *et al.* [8] report the top diameter of their scaled furnace is 274 mm, the belly has a diameter of 430 mm, and two outlets are located at the bottom sides with equal size of 35 mm. The height of the scaled furnace is 800 mm.

Table 2. Dimension comparison [m]

Reference	Height	Inlet	Outlet	Shaft	Belly	Deadman height
Zhang et al.	0.8	0.274	0.035	0.513	0.430	
Safavi Nick et al.	20	6.7	2.15	12.1	10.6	2.5

Zhang *et al.* [8] has also carried out an experimental study on a laboratory scaled furnace, where a glass bed is used to represent the burden in an actual furnace. The density, diameter and volume fraction which have been used in their study are equal 2500 kg/m^3, 3 mm and 0.58 respectively. **Table 3** shows a comparison between materials properties for the two cases.

Table 3. Material properties comparison

Ref	Density [kg/s]	Volume fraction	Diameter [m]
Zhang et al.	2500	0.58	0.003
Safavi Nick et al.	3700	0.68	0.015

Zhang *et al.* [8] reported the velocity field for a solid phase for three different cases:

- Case ‘a’ shows the velocity field when the solid mass flow rate is equal to 3.33×10^{-3} kg/s for a zero gas flow rate.
- Case ‘b’ shows the same quantity for a solid mass flow rate equal to 6.67×10^{-3} kg/s with a zero gas flow rate.
- Case ‘c’ shows the result for a solid mass flow rate of 3.33×10^{-3} kg/s and for a gas flow rate equal to 5.97×10^{-3} kg/s.

The comparison has been done between case ‘a’ of their model with the third case in the current study. Here, ε_s is equal to 0.68 in this study which is shown in **Figure 9**. At a first glance, it can be said that

in Zhang *et al.*'s [8] case the velocity at the top of the furnace (solid inlet area at the throat) is lower than the velocity at the outlet at the bottom of the domain. On the other hand, **Figure 9** of the current study shows that magnitude of solid phase velocity at the top of the furnace is higher than at the outlet area. To be able to explain the difference, the ratio of the outlet area to inlet area must be calculated for both cases. The ratio of the outlet area to inlet for the laboratory scaled furnace is:

$$\left.\frac{A_{outlet}}{A_{inlet}}\right|_{Zhang\ et\ al.} = 0.6214$$

while this value for the current full scaled operational blast furnace used in this study is:

$$\left.\frac{A_{outlet}}{A_{inlet}}\right|_{Safavi\ Nick\ et\ al.} = 1.3178$$

As can be seen, the area of the inlet in the current study is smaller than the outlet. However, for the laboratory scale geometry the situation is reverse. The velocity has an inverse relation to the area for a constant mass flow rate. Therefore, the velocity at the top of Zhang *et al.* [8] model is smaller than at the outlet area then. This is due to the larger inlet area. However, in the current study the area of the inlet is smaller than the area of the outlet. This results in an increased velocity magnitude at the top of the furnace in comparison to at the outlet area.

Contour lines are also drawn in Zhang *et al.* [8] study. The contour lines at the shaft show a small curvature around the symmetry axes. The same behavior can be seen in **Figure 9** for the current study. However, the magnitude of the velocity changes is smaller than in the current study. It can be seen that in the current study the velocity at slab 45 above the belly region is approximately 5.7×10^{-5}, while this value is 9.5×10^{-5} at the top of the furnace. This can be due to the characteristic of the deadman. The height of the deadman in Zhang *et al.* [8] laboratory scale study with respect to the furnace height is:

$$\left.\frac{h_{deadman}}{h_{furnace}}\right|_{Zhang\ et\ al.} = 0.4$$

The same value for the current full scaled blast furnace domain is:

$$\left.\frac{h_{deadman}}{h_{furnace}}\right|_{Safavi\ Nick\ et\ al.} = 0.15$$

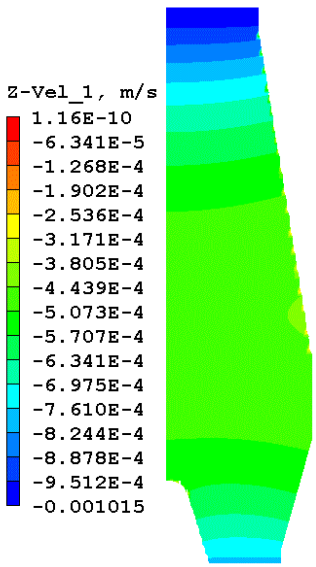

Figure 9 Contour plot of solid phase velocity profile with solid volume fraction equal to 0.68

It should also be added that the deadman height goes over the belly region of the furnace into the shaft in the laboratory scale study. However, in the current study the height of the deadman does not even reach the belly region of the furnace. Furthermore, above the deadman the peak the velocity decreases to 8.5×10^{-5} in Zhang *et al.*'s [8] study, which is almost six times smaller than the inlet value. However, the peak velocity value in the current study is around 4.4×10^{-5}which represents almost half the magnitude of the inlet velocity.

To summarize the comparison, it should be said that there are considerable differences between the furnace geometry in Zhang *et al.*'s [8] study and the current study with respect to the area of the inlet and outlet. Moreover, the difference in the size of the deadman between these two studies must be emphasized. On the other hand, the velocity contour lines at the shaft show a curvature in both cases. The magnitude of velocity at the top of the deadman decreases due to a blockage at the region of the deadman for both cases, but the decreasing rates are different. Both cases show an increase in the magnitude of the velocity close to the outlet of the domain.

Intentionally left blank!

5 Conclusion

A mathematical model based on the concept of continuum mechanics has been developed. It assumes that the existing phases in a blast furnace behave as a continuum media. Hence, the Navier-Stokes differential equation was used to describe the system and it was solved for two-phase solid-gas system in three-dimensional domain. The geometry was based on one of the SSAB's operational furnace located in Oxelösund, Sweden. Since, the solid particles are not exactly a continuum media, extra terms should be added to the Navier-Stokes equation. Therefore, the concept of the solid surface stress was added to the original differential equation to describe the interactions between particles due to packing including normal and shear forces.

The results showed that the additional extra terms in the Navier-Stokes equation behave as a breaking force in the continuum model to simulate the particle-particle interaction due to collision and packing. The profile of the deadman has been assumed to have a specified shape and size. It was shown that the solid particles have a 'V' shape profile at the top of the furnace and they follow the same profile from the throat up to the belly. However, during the descending in the furnace they are affected by the characteristic of the deadman after the belly region. In this region, their velocity profiles change from a 'V' shape to a 'W' shape. It was also shown that an increase in the compaction modulus increases the effective pressure. An increase in the effective pressure increases the magnitude of the surface stress tensor. This, in turn, reduces the velocities magnitude and affects the velocity profiles accordingly.

The volume fraction of solid particles plays an important role in the blast furnace. Therefore, the influence of three different packing densities (0.68, 0.71 and 0.74 respectively) on the profile of the flow through the upper part of the blast furnace from the throat to the tuyeres level was studied. Maximum velocity contours were calculated for the different packing densities in a production scaled furnace. It is shown that the particles velocity increases in the upper part of the furnace (from the throat down to the tuyeres) with a decrease in the packing density (from 0.74 to 0.71and 0.68), while keeping all other parameters constant. The shrinkage in size of the particles is not applied to the model. However, it is plausible to say that an increase in the packing density of the bed decreases the velocity magnitude. This, in turn, increases the resident time of the particles in the blast furnace.

The results are also compared with data from a laboratory scale furnace, where the ratio of inlet to outlet is doubled between the laboratory scaled model to the current production scale furnace. The comparison revealed that the velocity magnitude is different, while the overall velocity profile seems to be similar. However, the velocity magnitude at the top of the deadman in the laboratory model and the current full-scale model are 3.8×10^{-5} [m/s] and 6.87×10^{-4} [m/s], respectively. The difference is deemed to be due to the material pressure, which is larger in a full-scale furnace compared to a laboratory-scale furnace.

Intentionally left blank!

6 References

[1] International Iron and Steel Institute: Steel Statistical Yearbook, 1989.
[2] Y. Omori, Blast furnace phenomena and modelling, Elsvier, London, 1987.
[3] J.-i. Yagi, ISIJ International, 33 (1993) 619-639.
[4] J. Chen, T. Akiyama, H. Nogami, J.-i. Yagi, H. Takahashi, ISIJ International, 33 (1993) 664-671.
[5] P.R. Austin, H. Nogami, J.-i. Yagi, ISIJ International, 37 (1997) 458-467.
[6] P.R. Austin, H. Nogami, J.-i. Yagi, ISIJ International, 37 (1997) 748-755.
[7] P.R. Austin, H. Nogami, J.-i. Yagi, ISIJ International, 38 (1998) 246-255.
[8] S.J. Zhang, a.B. Yu, P. Zulli, B. Wright, U. Tüzün, ISIJ International, 38 (1998) 1311-1319.
[9] K. Takatani, T. Inada, Y. Ujisawa, ISIJ International, 39 (1999) 15-22.
[10] J.A.D. Castro, H. Nogami, J.-i. Yagi, ISIJ International, 40 (2000) 637-646.
[11] J.A.D. Castro, H. Nogami, J.-i. Yagi, ISIJ International, 41 (2001) 18-24.
[12] J.A.D. Castro, H. Nogami, J.-i. Yagi, ISIJ International, 42 (2002) 44-52.
[13] J.A.D. Castro, H. Nogami, J.-i. Yagi, ISIJ International, 42 (2002) 1203-1211.
[14] S.J. Zhang, A.B. Yu, P. Zulli, B. Wright, P. Austin, Applied Mathematical Modelling, 26 (2002) 141-154.
[15] H. Nogami, J.-i. Yagi, ISIJ International, 44 (2004) 1826-1834.
[16] S.S. Mondal, S.K. Som, S.K. Dash, Journal of Physics D: Applied Physics, 38 (2005) 1301-1307.
[17] X. Dong, A. Yu, J.-i. Yagi, P. Zulli, ISIJ International, 47 (2007) 1553-1570.
[18] X.F. Dong, a.B. Yu, J.M. Burgess, D. Pinson, S. Chew, P. Zulli, Industrial & Engineering Chemistry Research, 48 (2009) 214-226.
[19] G.L. Qing, L. Ma, X.S. Zhang, J.L. Zhou, M. Kuwabara, Ironmaking & steelmaking, 37 (2010) 546-552.
[20] S. Ueda, S. Natsui, H. Nogami, J.-i. Yagi, T. Ariyama, ISIJ International, 50 (2010) 914-923.
[21] J.A. de Castro, A.J. da Silva, Y. Sasaki, J.-i. Yagi, ISIJ International, 51 (2011) 748-758.
[22] H. Kawai, H. Takahashi, ISIJ International, 44 (2004) 1140-1149.
[23] T. Nouchi, T. Sato, M. Sato, K. Takeda, T. Ariyama, ISIJ International, 45 (2005) 1426-1431.
[24] Z. Zhou, H. Zhu, A. Yu, B. Wright, D. Pinson, P. Zulli, ISIJ International, 45 (2005) 1828-1837.
[25] H.P. Zhu, Z.Y. Zhou, a.B. Yu, P. Zulli, Granular Matter, 11 (2009) 269-280.
[26] S. Natsui, S. Ueda, M. Oikawa, Z. Fan, J. Kano, R. Inoue, T. Ariyama, ISIJ International, 49 (2009) 1308-1315.
[27] S. Natsui, S. Ueda, Z. Fan, N. Andersson, J. Kano, R. Inoue, T. Ariyama, ISIJ International, 50 (2010) 207-214.
[28] Z.Y. Zhou, H.P. Zhu, B. Wright, a.B. Yu, P. Zulli, Powder Technology, 208 (2011) 72-85.

[29] Z. Fan, S. Igarashi, S. Natsui, S. Ueda, T. Yang, R. Inoue, T. Ariyama, ISIJ International, 50 (2010) 1406-1412.
[30] Z. Fan, S. Natsui, S. Ueda, T. Yang, J. Kano, R. Inoue, T. Ariyama, ISIJ International, 50 (2010) 946-953.
[31] P.A. Cundall, O.D.L. Strack, Géotechnique, 29 (1979) 47-65.
[32] D. Kolymbas, Archive of applied mechanics, 61 (1991) 143-151.
[33] G. Gudehus, Soils and Foundations, 36 (1996) 1-12.
[34] S.A. Zaïmi, T. Akiyama, J.-B. Guillot, J.-I. Yagi, ISIJ International, 40 (2000) 322-331.
[35] S.A. Zaïmi, T. Akiyama, J.-B. Guillot, J.-I. Yagi, ISIJ International, 40 (2000) 332-341.
[36] S.a. Zaïmi, J.-B. Guillot, H. Biausser, Ironmaking and Steelmaking, 30 (2003) 475-482.
[37] I. Goldhirsch, Powder Technology, 182 (2008) 130-136.
[38] S.P.E. Forsmo, J.P. Vuori, Powder Technology, 159 (2005) 71-77.
[39] R.M. German, Particle Packing Characteristics, Princeton, New Jersey, 1989.
[40] K. Runesson, L. Nilsson, Bulk Solids Handling, 6 (1986) 877-884.
[41] P.C. Johnson, R. Jackson, Journal of Fluid Mechanics, 176 (1987).
[42] P.C. Johnson, P. Nott, R. Jackson, Journal of Fluid Mechanics, 210 (1990) 501-535.
[43] K. Hutter, K.R. Rajagopal, Continuum Mechanics and Thermodynamics, 6 (1994) 81-139.
[44] S.B. Savage, in: J.T. Jenkins, M. Satake (Eds.) U.S./Japan seminar on new models and constitutive relations in the mechanics of granular materials, Elsevier, New York, 1983.
[45] S. Ergun, Chemical Enginerring progress, 48 (1952) 89-94.
[46] J. Richardson, W. Zaki, Trans.Inst.Chem.Eng., 32 (1954) 35-53.
[47] H. Norem, in: the Davos Symposium, Avalanche Formation, Movements and Effects, IAHS, 1987, pp. 363-380.
[48] C. Orr, Particulate Technology, Macmillan, New York, 1966.
[49] M. Swartling, in: Applied Process Metallurgy, KTH Royal Institute of Technology, Stockholm, 2006.
[50] S.M. Eldighidy, R.Y. Chen, R.A. Comparin, Journal of Fluids Engineering, 99 (1977) 365-370.
[51] M. Gad-el-Hak, Journal of Fluids Engineering, 121 (1999).
[52] P.H. Gaskell, A.K.C. Lau, International Journal for Numerical Methods in Fluids, 8 (1988) 617-641.
[53] D.B. Spalding, Numerical computation of multi-phase fluid flow and heat transfer, in: C. Taylor, M. Morgan (Eds.) Recent advances in numerical methods in fluids, Pineridge Press, Swansea, 1980, pp. 139-167.